Ecosystems (2006) 9: 288–304
DOI: 10.1007/s10021-005-0146-y

ECOSYSTEMS

Identifying Differences in Carbon Exchange among Arctic Ecosystem Types

M. Williams,[1]* L. E. Street,[1] M. T. van Wijk,[2] and G. R. Shaver[3]

[1]*School of GeoSciences, University of Edinburgh, crew Building, Edinburgh, EH9 3JN, UK;* [2]*Plant Production Systems, Wageningen University, Plant Sciences, Haarweg 333, 6709 RZ, Wageningen, The Netherlands;* [3]*The Ecosystems Center, Marine Biological Laboratory, Woods Hole, Massachusetts 02543, USA*

Abstract

Our objective was to determine *how varied* is the response of C cycling to temperature and irradiance in tundra vegetation. We used a large chamber to measure C exchange at 23 locations within a small arctic catchment in Alaska during summer 2003 and 2004. At each location, we determined light response curves of C exchange using shade cloths, twice during a growing season. We used data to fit a simple photosynthesis-irradiance, respiration-temperature model, with four parameters. We used a maximum likelihood technique to determine the acceptable parameter space for each light curve, given measurement uncertainty. We then explored which sites and time periods had parameter sets in common—an indication of functional similarity. We found that seven distinct parameter sets were required to explain observed C flux responses to temperature and light variation at all sites and time periods. The variation in estimated maximum photosynthetic rate (P_{max}) was strongly correlated with measurements of site leaf area index (LAI). The behavior of tussock tundra sites, the dominant vegetation of arctic tundra, could largely be described with a single parameter set, with a P_{max} of 9.7 μmol m^{-2} s^{-1}. Tussock tundra sites had, correspondingly, similar LAI (mean = 0.66). Non-tussock sites (for example, sedge and shrub tundras) had larger spatial and temporal variations in both C dynamic parameters (P_{max} varying from 9.7–25.7 μmol m^{-2} s^{-1}) and LAI (0.6–2.0). There were no clear relationships between dominant non-tussock vegetation types and a particular parameter set. Our results suggest that C dynamics of the acidic tussock tundra slopes and hilltops in northern Alaska are relatively simply described during the peak growing season. However, the foot-slopes and water tracks have more variable patterns of LAI and C exchange, not simply related to the dominant vegetation type.

Key words: carbon flux; leaf area index; tundra; landscape heterogeneity; net ecosystem exchange; photosynthesis; respiration; maximum likelihood analysis.

Introduction

The Arctic contains large stores of C, predominately in soils, and there is debate on whether it is currently a source or a sink of C (Shaver and others 1992; Oechel and others 1993, 2000). Global change is already affecting the climate and vegetation structure of arctic regions (Oechel and others 2000), and, because they are likely to warm more than lower latitudes, their response to warming may be more rapid and significant than in other biomes. Atmospheric inversion studies suggest the presence of large C sinks in the northern hemisphere (Gurney and others 2002). However,

Received 2 November 2004; accepted 20 January 2005; published online 15 March 2006.
Corresponding author; e-mail: mat.williams@ed.ac.uk

detailed studies of ecosystem C exchange by eddy covariance at tundra sites have not proved conclusive (Vourlitis and Oechel 1997, 1999).

A key problem in determining regional carbon budgets lies in using detailed data from only a few measurement sites to determine activity in the larger, surrounding landscape. For instance, eddy flux towers (Baldocchi 2003) are a common method of assessing C exchange from a footprint upwind of the tower. Typically the footprint extends over approximately 1 km^2. The expense of tower operations means that such data are sparse. However, models of vegetation C exchange can be parametrized and tested against flux data (Williams and others 2000). Model parameters and drivers can be generated in a grid over the surrounding region, and the model run for each grid cell to produce an estimate of C exchange (Williams and others 2001). This approach is typical of most upscaling methodologies. There are problems with this approach, ranging from the reliability of the flux data and the generality of the model, to the generation of landscape drivers, such as leaf area index (LAI).

The scales of analysis and calculation used in upscaling are generally imposed by the techniques employed. For example, remote sensing data on vegetation cover is derived from satellites with spatial resolutions of approximately 1 km^2, similar in size to the footprint of flux tower data. But Williams and others (2001) show a poor correlation between LAI measured in destructive harvests in arctic tundra in 0.2 × 0.2 m quadrats versus normalized difference vegetation index (NDVI) data from satellites at 1 km^2 resolution. Arctic vegetation varies on finer spatial scales than 1 km^2, correlating to variations in topography, hydrology and frost-heaves (Shaver and others 1996). Flux tower and satellite data are complex, composite signals of the activity of multiple vegetation types.

Studies in the Arctic have already demonstrated the importance of vascular plant activity in controlling CO_2 fluxes (Williams and others 2000; McFadden and others 2003). Also, simple models of photosynthesis and respiration have been shown to make reliable predictions of net ecosystem exchange (NEE) in moist tundra (Vourlitis and others 2000). Here, we describe a detailed study of C exchange in an arctic upland catchment over two growing seasons. Our objective was to determine *how varied* is the response of C cycling to temperature and irradiance. Could all observations along a toposequence be described by a single parameterization of a light curve and temperature response function? This is unlikely, as variations of structure along toposequences are well-known (Shaver and others 1996). But what is not known, and has not been examined before, is whether a toposequence requires 3 or 30 different parametrizations to explain observed responses. We also aimed to determine if there was a gradual change in parametrizations or whether there were sharp boundaries in process, coincident with dominant vegetation types. This spatio-temporal information on process is critical for efforts to scale up observations of ecosystem process to generate landscape-level estimates.

Methods

The Study Area

The Imnavait Creek catchment (68°37′N 149°18′W, ~930 m a.s.l.) is situated north of the Brooks Range in the Southern Arctic foothills physiographic sub-province of the Alaskan North Slope (Walker 1994). The creek itself is a first-order stream, a small beaded tributary of the Kuparuk River, which runs north from its headwaters in the Brooks Range to the Arctic Ocean. The 2.2 km^2 catchment is representative of the surrounding landscape of rolling hills, rising less than 100 m from valley bottom to hilltop. The slopes are dominated by graminoid tussock tundra, which is the major vegetation type in the circumpolar tundra zone. Soils are mainly 0.15–0.2 m of porous organic matter underlain by silt and glacial till, with thaw depths ranging from 0.25 to 1.0 m (Hinzman and others 1991). Snow melt occurs in early May to late June and the snow season returns in September, allowing only a short growing season. The mean annual precipitation and mean annual air temperature at Imnavait from 1985 to 1993 were 340 mm and −7.4°C respectively (Stieglitz and others 2000).

During summer 2003, eight flux measurement plots were situated along the topographic sequence of the west-facing slope of Imnavait creek catchment. In the summer of 2004, 15 flux plots were set out along the same topographic sequence. Vegetation along this sequence varies from dry heath communities on the ridge through graminoid dominated tussock tundra on the mid-slopes, to shrub dominated tussock tundra and sedge meadow on the wetter foot-slopes (Table 1). Gradients in vegetation also exist moving across the slope in between water tracks, which drain the west face approximately every 10 m. Well-defined water tracks have distinctive margins of *Salix pulchra*, grading into *Betula nana*

Table 1. Description of Flux Measurement Plots

Vegetation Type	Code	Position	Dominant Vascular Plant Species	Sampling Year
Betula (dry)	3B	Foot-slope	*B. nana, V. vitis-idaea*	2003
Betula Water Track	3BW	Upper Back-slope	*B. nana, V. vitis-idaea, Eriophorum* spp.	2003
Hilltop Heath	3HH	Shoulder	*Arctostaphylos alpina, V. vitis-idaea, V. uliginosum*	2003
Wet Sedge	3S	Foot-slope	*Carex* spp. *Eriophorum* spp.	2003
Tussock (hilltop)	3TH	Crest	*Eriophorum* spp. *L. palustre, V. vitis-idaea.*	2003
Tussock (open)	3TO	Lower Back-slope	*Eriophorum* spp., *L. palustre, Cassiope tetragona*	2003
Tussock (wet)	3TW	Foot-slope	*Eriophorum* spp., *V. vitis-idaea, B. nana, Ledum palustre*	2003
Salix Water Track	3X	Foot-slope	*Salix pulchra, Vaccinium vitis-idaea, Betula nana, Rubus chamaemorus*	2003
Betula (dry)	4B1	Mid-slope	*B. nana, V. vitis-idaea, L. palustre*	2004
Betula (wet)	4B2	Foot-slope	*B. nana, R. chamaemorus, V. vitis-idaea*	2004
Betula (wet)	4B3	Foot-slope	*B. nana, V. vitis-idaea, L. palustre*	2004
Rubus	4R1	Foot-slope	*R. chamaemorus, Salix* spp.	2004
Rubus	4R2	Foot-slope	*R. chamaemorus, Salix* spp.	2004
Wet Sedge	4S1	Foot-slope	*Carex* spp. *Eriophorum* spp., *Andromeda polifolia*	2004
Wet Sedge	4S2	Foot-slope	*Carex* spp. *Eriophorum* spp., *R. chamaemorus, Salix* spp.	2004
Tussock	4T1	Upper Back-slope	*Eriophorum* spp., *V. vitis-idaea, L. palustre, B. nana*	2004
Tussock	4T2	Upper Back-slope	*V. vitis-idaea, Eriophorum vaginatum, L. palustre, C. tetragona, B. nana*	2004
Tussock	4T3	Upper Back-slope	*B. nana, L. palustre, V. vitis-idaea, Carex* spp., *R. chamaemorus*	2004
Tussock	4T4	Upper Back-slope	*Carex* spp., *V. vitis-idaea, L. palustre, B. nana, Salix* spp., *E. vaginatum*	2004
Tussock	4T5	Lower Back-slope	*Carex* spp., *V. vitis-idaea, E. vaginatum, B. nana, L. palustre*	2004
Salix (dry)	4X1	Foot-slope	*Empetrum nigrum, V. vitis-idaea, Salix* spp., *B. nana, C. tetragona*	2004
Salix Water Track	4X2	Foot-slope	*B. nana, Salix* spp., *R. chamaemorus, V. vitis-idaea, Carex* spp.	2004
Salix Water Track	4X3	Foot-slope	*Salix* spp., *R. chamaemorus*	2004

Position given is the judged position relative to Walker and Walker's (1996) idealized toposequence along the west-facing slope of Imnavait. Dominant vascular plant species are those with the greatest number of leaf hits from point intercept sampling (Shaver and others 2001), and are listed in dominance order.

communities, which separate the water track vegetation from graminoid tussock tundra in-between. Vegetation types are described in detail in Walker and Walker (1996) and Walker and others (1994).

Gaseous CO_2 Measurement

Carbon exchange measurements could not be made simultaneously along the toposequence. Any inter-comparison of C exchange between plots or time periods is obfuscated by the differences in ambient environmental conditions. Our solution to this problem was to measure C exchange at each plot with artificial variations in light intensity (that is, to generate light-response curves), and to record air temperature during each measurement. We fitted the observations to a simple net ecosystem production model, incorporating the light response of photosynthesis and a temperature response of respiration. Given measurement uncertainty, we statistically compared the fitted model parameter sets between plots and time periods, to determine how many distinct parameter sets were required to characterize the landscape.

We subjectively selected twenty-three 1 m × 1 m plots representing different homogenous vegetation types along the topographic sequence with replication (Table 1). We completed two flux measurement periods in 2003 (5th–10th July and 19th–24th July) and two in 2004 (12th–17th July and 4th–14th August). The usual sequence at a plot involved measurement firstly under ambient light, followed by three increasing levels of shading, followed by a dark measurement. The chamber was shaded by layering three net cloths and was covered with tarpaulin to achieve complete darkness. We repeated this measurement series 4–5 times throughout the day at each plot in 2003 and 2–3 times in 2004. We collected 672 independent chamber estimates of CO_2 fluxes over the 2 years.

We measured CO_2 flux using a Li-Cor 6400 (Li-Cor Inc., Lincoln, Nebraska, USA) connected to a 1 m × 1 m × 0.25 m Plexiglas chamber which was fitted over a chamber base. The chamber base was supported several centimeters above the ground surface by steel legs driven down to the permafrost. We sealed the chamber base to the ground by weighting plastic sheeting attached to the bottom rim of the base. This provided a good seal by depressing the plastic sheeting into the wet moss surface. The Li-Cor 6400 recorded CO_2 and H_2O concentration in the chamber over 30 s. Photosynthetic photon flux density (PPFD) and chamber air temperature were also monitored by the Li-Cor.

We calculated fluxes from chamber concentrations recorded by the Li-Cor 6400 according to the formula

$$F_C = \frac{\rho V \mathrm{d}C/\mathrm{d}t}{A}, \qquad (1)$$

where F_c is net CO_2 flux (μmol m^{-2} s^{-1}), ρ is air density (mol m^{-3}), V is the chamber volume (m^3), $\mathrm{d}C/\mathrm{d}t$ is the slope of chamber CO_2 concentration against time (μmol mol^{-1} s^{-1}) and A is the chamber surface area (m^2). To calculate an accurate chamber volume, we recorded a grid of 36 depth measurements from the top of the chamber base to the ground surface, at the beginning and end of each day.

Vegetation Characterization

In each flux plot we took 25 readings over a regular grid with a Li-Cor LAI-2000 Plant Canopy Analyzer (Li-Cor Inc., USA). We also took 25 readings to determine the NDVI of each flux plot, using a portable two-channel light sensor (Skye Instruments Ltd, Llandrindod Wells, UK). NDVI was calculated by the formula;

$$\mathrm{NDVI} = (R_{\mathrm{IR}} - R_{\mathrm{VIS}})/(R_{\mathrm{NIR}} + R_{\mathrm{VIS}}) \qquad (2)$$

where R_{NIR} is reflectance at a wavelength of 0.725–1.0 μm and R_{VIS} is reflectance at 0.58–0.68 μm. We repeated these observations during each measurement period. To use the NDVI and LAI-2000 as an indicator of real LAI of the flux plots, we produced calibration curves using data from thirty 0.2 m × 0.2 m harvests. These harvests were taken at Imnavait Creek watershed (two by each 2003 flux plot) and near Toolik Lake Field Station in 2003. We measured the LAI (via LAI-2000) and NDVI of each harvest plot before removing all vascular plant material. In the lab we separated leaf material and determined LAI destructively, sorted by species, using a scanner and the software package WinRhizo (Regent Instruments Inc, Ste-Foy, Canada).

We also characterized the vegetation of each plot by point intercept sampling. Each flux plot was sampled using a 0.7 m × 0.7 m frame with a grid of 100 points. For each pin drop we recorded the total number of stem and leaf hits for each species as well as the canopy height.

Analysis of Flux Data

We modelled NEE of CO_2 by a combined representation of photosynthetic irradiance-response

and temperature-sensitive respiration, using a four-parameter model (the PIRT model):

$$\mathrm{NEE} = R_b e^{\beta T} - \frac{P_{max} I}{k + I}, \quad (3)$$

where P_{max} is the rate of light saturated photosynthesis (μmol CO_2 m^{-2} s^{-1}), k is the half-saturation constant of photosynthesis (μmol PAR m^{-2} s^{-1}), I is the incident PPFD (μmol m^{-2} s^{-1}), R_b is basal ecosystem respiration (μmol CO_2 m^{-2} s^{-1} at 0°C), and β quantifies the relative increase in respiration with air temperature, T (1/°C). In a separate exercise, we also fitted the first term in the right-hand side of equation (3) (the RT model) to dark respiration data alone. The PIRT and RT model parameters were thus determined separately.

Initially, we determined unknown parameters for PIRT and RT models by minimizing the root-mean-square error (RMSE) of predictions versus observations using a quasi-Newton method and finite difference gradient (UMINF routine, IMSL, Visual Numerics, Houston, Texas, USA). But because of uncertainties in the observations, we also used the maximum likelihood technique (MLT, van Wijk and Bouten 2002) to estimate the unknown parameters of the model. Maximum likelihood estimators properly represent measurement error, and so provide a statistically sound basis for determining the adequacy of a model fit, and for finding the multivariate parameter confidence region. The optimal parameters are found by minimizing the objective function

$$O(p) = \sum_{i=1}^{n} \frac{1}{\sigma_{Yi}^2} \left[y_{i,\mathrm{meas}}(x_i) - y_{i,\mathrm{mod}}(x_i : p) \right]^2, \quad (4)$$

where n is the total number of measurements, p is the number of model parameters, $y_{i,\mathrm{meas}}(x_i)$ is the measured value of output variable y at the value x_i of the driving variable x, $y_{i,\mathrm{mod}}(x_i{:}p)$ is the modelled value of the output variable at the value x_i of the driving variable x given the parameters p, and σ^2_{yi} is the measurement error variance for each of the observations. The minimal sum-of-squares follows a chi-squared (χ^2) distribution with n-p degrees of freedom.

We used a Monte–Carlo approach to generate parameter confidence regions. For the PIRT model, we determined the value of the objective function for combinations of all four parameters at 40 points linearly arranged between specified maximum and minimum values [$1 < P_{max} < 30$, $100 < k < 1000$, $0.1 < R_b < 3$, $0.01 < \beta < 0.2$, for units see equation (3)]. We used a χ^2 test to determine which of the 2.56×10^6 combinations for each data-set lay within a 95% confidence interval of the observations. The degrees of freedom was determined as n–p, where n is the number of observations and p is the number of model parameters. For the RT model, we determined the value of the objective function for combinations of both parameters (R_b and β) at 100 points between the same bounds used in the PIRT model.

To estimate parameter confidence regions, the error in the data must be specified. We estimated the measurement error variance of the chamber technique by comparing measurements taken under similar conditions on the same day. We compared estimates of NEE determined (1) at light levels with a range less than 100 μmol PAR m^{-2} s^{-1}, (2) at light levels greater than 1,000 μmol PAR m^{-2} s^{-1}, or (3) under conditions of total darkness. We always ensured a comparison of three or more data points to generate variance estimates, and we noted the variation in temperature between each measurement point. We used 2003 data only for this exercise, because more data were collected at each site during this field campaign.

Using the MLT, for the 23 sites and two time periods, we attempted to identify 46 sets of acceptable parameter combinations for the PIRT model. We combined data from the two measurement periods at each site to determined 23 sets of acceptable parameter combinations for the RT model via the MLT. For both PIRT and RT models and parameter spaces we then undertook two analyses. Firstly, for each site-specific (RT) or site and time-specific (PIRT) acceptable parameter combinations, we checked for parameter overlap between sites and/or time periods. This analysis determines whether the same model and same parameter combination can explain observed behavior at two different sites and/or time periods. If true, then there is no significant difference in light and temperature response of C exchange. In the second analysis, we determined the smallest number of parameter combinations that, together with PIRT or RT model, could explain all observed fluxes at all sites and time periods, given measurement uncertainty. This second analysis quantifies the functional heterogeneity of C dynamics in terms of light and temperature responses.

Analysis of Vegetation Data

We only collected indirect measurements of leaf area at the flux plots. To calibrate the indirect methods, we generated relationships between the indirect techniques and direct, harvest measurements of LAI (n = 30). For the NDVI data (N), we

used an exponential model to relate LAI (L) to NDVI, with two unknown parameters, a and b,

$$L = a\exp(b \cdot N). \quad (5)$$

For the LAI-2000 data (L_{2000}) we used a linear model with parameters c and d,

$$L = c + dL_{2000}. \quad (6)$$

We used the MLT to estimate the unknown parameters [equation (4)]. We estimated that measurement uncertainty on the destructive harvests, and also related to mismatches between the sampling of direct and indirect methods, had a base error of 0.1 m^2 m^{-2}, plus 5% of harvest LAI. We used the complete set of acceptable parameters from the MLT to determine the standard deviation (σ) on the estimate of LAI obtained using NDVI. The standard error of the LAI estimate for the 1 m × 1 m plot was calculated as $\sigma/\sqrt{n}$, where n = 25.

Results

Flux Measurement Errors

The mean error on all dark chamber replicates was 0.49 μmol m^{-2} s^{-1} (Table 2), and we used this value for finding acceptable parameter sets for the RT model. There were three data sets where dark respiration data were replicated three times, and the range of air temperature was less than 1°C. The mean variance from the three data sets was 0.44 μmol m^{-2} s^{-1} (data not shown). There was no evidence of a correlation between temperature range and the magnitude of variance among dark respiration observations.

In 2003, for 12 of the 16 measurement periods, we were able to select 3–5 data points recording NEE under light conditions within a range of 100 μmol PAR m^{-2} s^{-1}. We used these data, and those for one site with radiance greater than 1,000 μmol m^{-2} s^{-1}, to estimate observational variance of 0.58 μmol m^{-2} s^{-1} (Table 2). The mean of the variances determined for all conditions (light and dark) was 0.53 μmol m^{-2} s^{-1}, and we used this value for finding acceptable parameter sets for the PIRT model using the MLT.

Ecosystem Respiration

The respiration data determined from dark chambers indicated a clear temperature response in CO_2 effluxes (Figure 1). Least squares fitting of the RT model at each site suggested a very broad range in basal rate (R_b), from 0.1 to 2.8 μmol m^{-2} s^{-1}, and also in temperature responses (β), from 0.01 to 0.19 (Table 3). However, there is a strong negative correlation (R^2 = 0.76) between the two sets of fitted parameters. The mean RMSE of model fitting to individual site data was 0.4 μmol m^{-2} s^{-1}.

Using the MLT, we found that, given measurement uncertainty, the RT model could generate clouds of acceptable parameters for the combined data at each site. We compared site-specific clouds in pairs to determine whether common parameters could explain activity at two different sites. In the 276 paired comparisons of the 23 data sets, we found that in 154 cases (56%) paired sites had parameter sets in common (Figure 2). Most sites had 8–18 parameters sets in common (Table 3).

Four sites were conspicuous in their measured respiratory behavior: 4X1, 4X2, 4S1, 4R2. These sites had parameters sets in common with just 0–3 other sites. Site 4X1 did not have acceptable parameter sets in common with any other site, and to explain the respiration data at the remaining 22 sites with the RT model required a minimum of five distinct, generic parameter sets (Figure 1, Table 4). Sites 4X2, 4S1 and 4R2 shared a generic parameter set, but it was unique to these three sites. However, 15 of the 23 sites could be simulated using a single parameter set (No. 3 in Table 4). Using these five generic parameter sets in place of the 23 best-fit sets, the mean RMSE of model fitting was 0.66 μmol m^{-2} s^{-1}, a 65% increase in estimation uncertainty.

Net Ecosystem Exchange of CO_2

Net ecosystem exchange of CO_2 had a clear response to light at all sites (Figure 3). Fitting the PIRT model by least squares indicated that maximum rates of photosynthesis varied between 6.6 and 30.0 μmol m^{-2} s^{-1}, half saturation points between 281 and 1,000 μmol m^{-2} s^{-1}, basal respiration between 0.1 and 1.7 μmol m^{-2} s^{-1}, and respiration-temperature coefficients between 0.0 and 0.18 (Table 5). Of the 46 curves, acceptable parameter sets were generated for 43. Data noise in measurements 3Xb, 4T1a and 4T2b prevented identification of any acceptable parameters. The mean RMSE of the PIRT model individually fitted to the 43 remaining measurements was 0.42 μmol m^{-2} s^{-1}.

In the 903 paired comparisons of the 43 available data sets, we found that in 482 cases (53%) sites had parameter sets in common (Figure 4). Most curves had parameters in common with more than 20 others, but three sites had just 5 in common: 4B2a, 4X1a and 4X2a. We examined the paired comparisons to see whether the photosynthetic

Table 2. Calculation of Error Values used in the Maximum Likelihood Analysis

Vegetation Type	Code	Mean NEP (variance) μmol m^{-2} s^{-1}	*n*	Mean PPFD (range) μmol m^{-2} s^{-1}	Mean Temp (range) °C	Mean VPD (range) KPa	Mean Respiration (range) μmol m^{-2} s^{-1}	*n*	Mean Temp. (range) °C
Betula (dry)	3Ba	−2.2 (0.48)	5	359 (98)	22.3 (3.7)	1.1 (0.42)	3.4 (0.15)	4	21.8 (4.1)
Betula (dry)	3Bb						2.8 (0.39)	5	19.9 (11.5)
Betula WT	3BWa	−4.4 (0.42)	4	468 (101)	25.0 (4.0)	1.4 (0.30)	2.3 (0.46)	5	18.0 (7.1)
Betula WT	3BWb	−4.6 (1.00)	3	1116 (640)	24.5 (2.8)	1.3 (0.17)			
Hilltop Heath	3HHa						1.7 (0.23)	4	21.7 (7.1)
Hilltop Heath	3HHb						2.1 (0.22)	3	23.3 (6.4)
Sedge	3Sa	−0.5 (0.26)	4	163 (52)	17.0 (0.2)	0.6 (0.15)	1.9 (0.13)	5	18.4 (10.5)
Sedge	3Sb	0.6 (0.06)	4	281 (19)	17.5 (3.2)	0.8 (0.45)	2.1 (0.08)	3	18.1 (2.4)
Tussock (hilltop)	3THa	−0.1 (0.35)	3	196 (26)	20.7 (7.3)	1.0 (0.96)	2.2 (0.23)	4	20.3 (7.9)
Tussock (hilltop)	3THb	−0.4 (0.24)	4	352 (72)	25.6 (5.2)	1.8 (0.71)	2.7 (0.83)	5	23.8 (7.9)
Tussock (open)	3TOa	−1.4 (0.42)	4	299 (89)	20.0 (5.1)	0.6 (0.42)	2.1 (0.23)	5	19.9 (8.5)
Tussock (open)	3TOb	0.7 (1.08)	4	203 (65)	25.0 (2.3)	1.4 (0.28)	3.1 (1.07)	4	24.6 (3.0)
Tussock (wet)	3TWa	−1.2 (1.00)	4	443 (95)	22.8 (3.5)	1.1 (0.42)	4.6 (0.72)	4	22.6 (3.5)
Tussock (wet)	3TWb	−1.7 (0.65)	4	256 (84)	22.2 (3.6)	1.0 (0.54)	3.1 (1.47)	5	20.0 (11.8)
Salix WT	3Xa	−0.6 (0.66)	4	146 (90)	16.8 (1.9)	0.7 (0.15)	2.7 (0.77)	6	18.8 (8.2)
Salix WT	3Xb	−6.3 (0.91)	3	231 (67)	16.2 (2.0)	0.6 (0.18)	2.4 (0.31)	5	16.8 (1.3)
Mean		−1.69 (0.58)					2.61 (0.49)		

The code identifies the site (see Table 1), with suffixes a and b indicating first or second time period of observation. Mean NEE and variance were determined from NEE data collected at a site either within a PAR range of 100 μmol m^{-2} s^{-1}, or at values greater than 1,000 μmol m^{-2} s^{-1}. The mean and range of PPFD (photosynthetic photon flux density), temperature and VPD (vapor pressure deficit) summarize the environmental conditions during NEE measurements. The mean and variance of respiration were determined by all flux observations collected in the dark during each time period. The mean and range of temperature conditions during the dark respiration measurements are provided. WT, water track; n, number of observations.

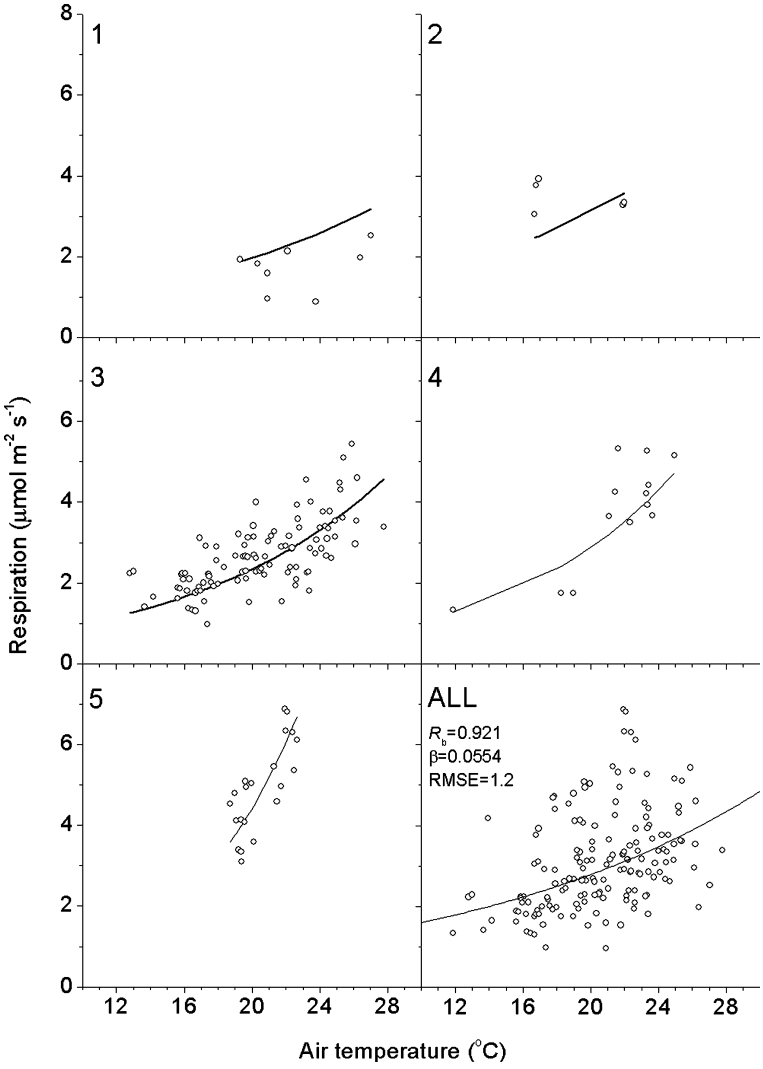

Figure 1. Ecosystem dark respiration (R_e) response to chamber air temperature. *Open symbols* shows measured ecosystem respiration C plotted against temperature. *Lines* show predictions of NEE using the RT model. The parameter set used in the RT model is indicated by the panel number, drawn from the five generic sets listed in Table 4. Full data are shown in *panel ALL*, while data are presently separately by site in *panels 1–5*, according to the generic parameter set that provides a statistically acceptable description for those data. For example, all non-wet tussock tundra sites are in *panel 3*. Where more than one generic parameter set was acceptable (Table 3) the commonest (first-listed) was selected. The parameters of the fit to all data are R_b = 0.92, β = 0.055, and the root-mean square error of prediction is 1.19.

light response and/or respiration temperature response changed over time at each site. In 14 out of 21 potential comparisons (sites 3X and 4T excluded, see above), the same parameters were acceptable for both periods, indicating there was no significant change over time (Table 5). For example, at the wet sedge site (3S) we found 38,839 acceptable parameter combinations for the PIRT model (out of a possible 2.56 million) could explain observations from period 1, and 86,660 acceptable combinations could explain observations from period 2. There were 20,344 combinations of parameters that could acceptably explain both data sets (Figure 5).

To explain C dynamics at all sites and time periods required a minimum of seven distinct, generic parameter sets for the PIRT model (Figure 3, Table 6). One single parameter set could explain 23 of the measured 43 curves. Using generic parameters, instead of the individually fitted parameters, resulted in a mean prediction RMSE of 0.70 μmol m^{-2} s^{-1}, an increase in estimation uncertainty of 66%. The parameter range for the generic sets was similar to that from the 43 individual fits. At 11 sites, a single generic parameter set could explain observations from both measurement periods, while at remaining sites there were significant changes in C exchange over time.

Analysis of Vegetation Data

For the 30 harvest plots, an LAI-NDVI model was able to explain 70% of the variation in harvest data, and the RMSE of LAI prediction was 0.35 (Figure 6). The LAI-2000 approach was able to explain 43% of LAI variation for all data (Figure 6), but there was a large positive intercept. Using the MLT, we attempted to find acceptable parameters relating the data to the models (equations 5, 6). We found acceptable parameter combinations relating

Table 3. Estimated Parameters of the Respiration-temperature Response Model

Vegetation Type	Code	R_b	b	Max. temp.	Min. temp.	n	RMSE	Grouped Parameter Sets	Grouped RMSE	Shared Parameter Sets
Betula (dry)	3B	1.51	0.034	24.5	13.0	9	0.40	3, 4, 2	0.70	17
Betula Water Track	3BW	0.30	0.109	25.9	13.7	7	0.48	3, 4, 2	0.74	17
Hilltop Heath	3HH	1.34	0.012	27.0	19.3	8	0.51	1	0.86	10
Wet Sedge	3S	1.62	0.010	23.3	12.8	8	0.32	3, 1	0.64	16
Tussock (hilltop)	3TH	0.55	0.067	27.8	16.9	9	0.49	3, 1	0.74	15
Tussock (open)	3TO	0.67	0.063	26.2	14.2	9	0.57	3, 1	0.62	15
Tussock (wet)	3TW	0.74	0.076	24.9	11.9	8	0.69	4, 2	0.81	12
Salix Water Track	3X	1.36	0.031	22.1	16.2	10	0.46	3, 4, 2	0.63	18
Betula (dry)	4B1	1.04	0.048	24.2	21.7	6	0.21	3, 4, 2	0.25	8
Betula (wet)	4B2	0.10	0.164	23.4	18.2	5	0.43	4	0.76	13
Betula (wet)	4B3	0.15	0.143	22.7	17.4	5	0.44	3, 4, 2	0.68	17
Rubus	4R1	2.83	0.010	22.0	16.7	6	0.35	2	0.84	12
Rubus	4R2	1.45	0.063	22.6	18.7	6	0.30	5	0.87	2
Wet Sedge	4S1	0.10	0.189	22.1	19.1	9	0.53	5	0.64	2
Wet Sedge	4S2	0.59	0.082	25.4	19.6	7	0.30	3, 4, 2	0.84	17
Tussock	4T1	0.78	0.053	22.6	15.6	6	0.18	3, 4, 1	0.32	18
Tussock	4T2	1.98	0.010	20.6	17.9	6	0.29	3, 4, 2	0.46	18
Tussock	4T3	0.66	0.067	24.9	19.5	7	0.26	3, 4, 2	0.29	18
Tussock	4T4	0.29	0.093	24.4	16.2	6	0.09	3, 1	0.50	16
Tussock	4T5	2.59	0.010	26.2	19.8	4	0.26	3, 1	0.69	16
Salix (dry)	4X1	2.76	0.010	23.0	17.8	9	0.93	None		0
Salix Water Track	4X2	2.28	0.036	21.7	19.6	6	0.39	5	0.67	3
Salix Water Track	4X3	0.60	0.084	23.5	15.9	5	0.21	3, 4, 2	0.88	18

R_b and β are fitted parameters. Max. temp and min. temp are the maximum and minimum air temperatures (T) recorded during measurements. n indicates the number of flux measurements of respiration at each site. RMSE is the root-mean-square error of the fitting process for individual data sets. Grouped parameter sets indicates which of the five generic parameter sets (Table 4) generate a statistically acceptable description of the temperature data at each site. The parameter set numbers are listed with the most generic parameter set first. Generic RMSE indicates the root-mean-square error of the fitting process using the first of the listed generic parameter sets. Shared parameter sets indicates the number of other sites that share acceptable model parameters.

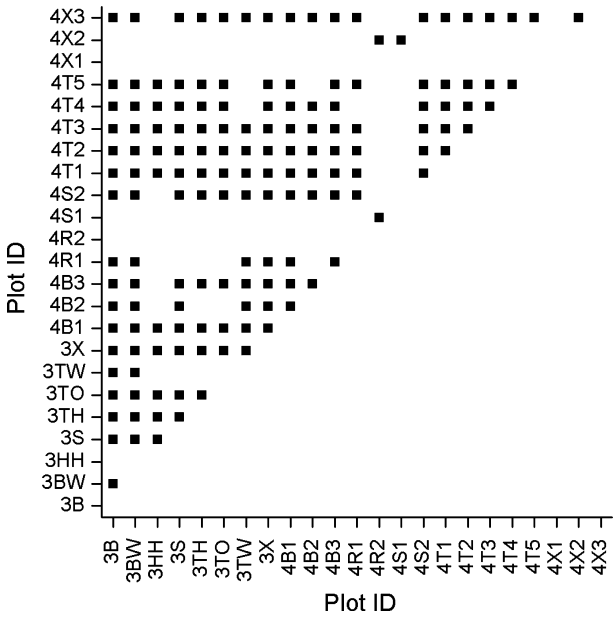

Figure 2. Common parameter analysis of the dark respiration-temperature model [$R_e = R_b \exp(\beta T)$] for each site. *Symbols* indicate when a single parameter set can acceptably model the respiration-temperature response observed at two sites. The *lack of a symbol* indicates that no common parameters were found (significant at 95% level). Data from periods 1 and 2 were combined for the analysis. Sites are identified by plot ID code; for details see Table 1.

the NDVI and LAI harvest data through the model (Figure 6). The errors on the modelling of LAI from NDVI data increase with LAI, with the errors increasing more rapidly with LAI greater than 1. We did not find any acceptable parameters relating the LAI-2000 data to the model.

We used the empirical models relating LAI to NDVI data to estimate the LAI in the 1 m × 1 m chamber plots. LAI tended to be highest in the *Salix*, *Rubus* and *Betula* dry sites (Table 5). LAI was lowest in wet sedge, open tussock and hilltop tussock. The greatest changes over time in LAI occurred in the *Rubus* and *Salix* sites monitored in 2004.

Discussion

Analysis of C Exchange Data

In analyzing the flux data, our goal was to identify significant differences in CO_2 exchange among sites and significant changes over the period of data collection, to determine the degree of heterogeneity of CO_2 exchange among tundra vegetation types. Full spatial heterogeneity exists when no single set of model parameters can explain CO_2 exchange for two vegetation types, given measurement uncertainty. Full spatial and temporal heterogeneity occurs when each vegetation type also requires separate parameters for each time period. Our expectation was that the catchment would be temporally homogeneous, and partially spatially heterogeneous according to dominant plant species distributions.

Table 4. Generic Parameter Sets for the Temperature Response Model

Generic set	R_b	β	Number of Sites Fitted
1	0.506	0.068	11
2	0.767	0.07	11
3	0.419	0.086	15
4	0.39	0.1	12
5	0.187	0.158	3

R_b and β are fitted parameters. The total number of sites where each generic parameter set is acceptable is also shown.

The analysis of the respiration data showed that most sites could be simulated by a single parametrization. Of the five generic parameter sets, four had similar temperature responses (parameter β) and a small range in basal respiration rate. The remaining generic parameter set (5) differed from the others primarily in its strong temperature response, and was required to explain observations at three sites (4X2, 4S1, 4R2). The unusual behavior at these sites (Figure 1) probably arose due to the small range in temperature (<4°C) that occurred during measurement (Table 3). The lack of any acceptable parameter sets at site 4X1 is probably also due to the small temperature range. Confirming that low temperature ranges confused the analysis, the replicated measurements on *Salix*, sedge and *Rubus* (3S and 4S2, 4R1, 3X and 4X3), all with larger temperature ranges during measurement, were explicable by generic parameter sets 2 and 3. These results suggest that patterns of ecosystem respiration have low variability among vegetation types. Also, given that at each site the RT model could always explain respiration data from both measurement periods with a single parametrization, there was no evidence of any change in respiration through the peak growing season.

The analysis of the full C exchange datasets showed that the light and temperature response for 43 out of 46 measurement sets could be explained with the PIRT model using seven distinct, generic parameter sets. Two of these parameter sets (1 and 3) had broad, largely shared applicability. Generic

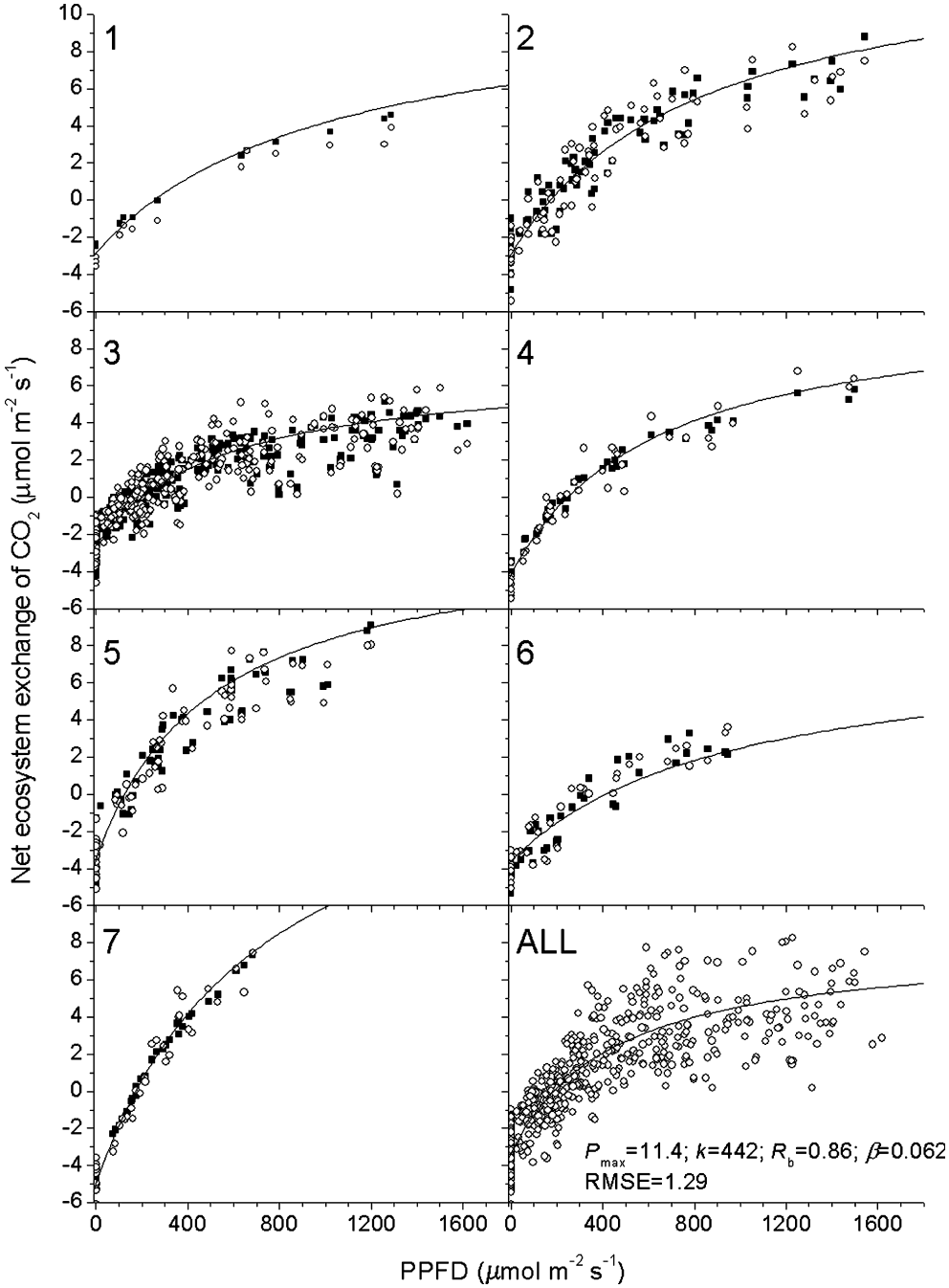

Figure 3. Relationships between measured net ecosystem exchange (NEE) of CO_2 and incident photosynthetic photon flux density (PPFD). *Open symbols* are measurements, *closed symbols* show predictions of NEE using the PIRT model. The full data are shown in *panel ALL*. In *panels 1–7*, data are shown and modelled separately, using a generic parameter set (Table 6) that provides a statistically acceptable description for those data. For example, all non-wet tussock tundra data are in *panel 3*. Where more than one generic parameter set was acceptable at a site and time period, the commonest (first-listed) parameter set was selected. The *lines* show the predicted NEE–PPFD response for each generic parameter set with a constant temperature of 22°C; model predictions vary from this line due to temperature changes. The parameters and root-mean square error (RMSE) for the fit to all data are listed.

parameter sets (PS) 1 and 3 could explain observations in all non-wet tussock and heath, and some sedge, *Salix* and *Betula* tundra. PS 2 could explain observations in eight cases, and was the only acceptable PS for some *Betula* tundra. PS 4 was a unique combination for wet tussock and some *Salix*

Table 5. Estimated Parameters for the PIRT Model for each Site and Time Period

Vegetation Type	Code	P_{max}	k	R_b	β	n	RMSE	Generic Parameter Sets	Generic RMSE	Shared Parameter Sets	LAI	Mean Temp. (°C)	Mean VPD (kPa)
Betula (dry)	**3Ba**	18.1	760	0.434	0.095	28	0.72	2	0.83	13	1.39	22.2	1.10
Betula (dry)	**3Bb**	14.6	581	0.100	0.153	11	0.51	2	0.61	17	1.15	21.3	0.96
Betula (WT)	**3BWa**	14.0	507	0.390	0.101	23	0.77	2	0.81	23	0.7	18.4	0.64
Betula (WT)	**3BWb**	14.0	590	0.247	0.117	17	0.63	2, 4	0.81	27	0.85	24.2	1.27
Hilltop Heath	**3HHa**	7.2	422	0.232	0.093	18	0.45	3	0.76	25	0.72	22.2	1.15
Hilltop Heath	**3HHb**	7.6	683	0.272	0.081	15	0.27	3	0.74	24	0.63	23.7	1.72
Sedge	**3Sa**	9.8	552	1.012	0.033	16	0.53	3, 1	0.74	24	0.65	17.8	0.69
Sedge	**3Sb**	13.5	623	0.466	0.079	16	0.27	3, 2	0.83	35	0.57	17.9	0.80
Tussock (hilltop)	**3THa**	8.0	452	0.996	0.033	20	0.55	3	0.81	24	0.46	21.8	1.10
Tussock (hilltop)	**3THb**	7.2	399	0.490	0.070	27	0.40	3	0.64	25	0.48	23.9	1.70
Tussock (open)	**3TOa**	11.4	611	0.527	0.076	23	0.36	3, 1	0.48	28	0.48	18.4	0.64
Tussock (open)	**3TOb**	9.3	471	0.102	0.140	21	0.47	3, 1	0.54	30	0.54	24.8	1.37
Tussock (wet)	3TWa	19.4	968	0.422	0.102	22	0.73	3, 1	0.82	13	0.94	22.8	1.06
Tussock (wet)	3TWb	19.4	685	0.914	0.062	17	0.43	4	0.74	13	0.97	21.4	0.99
Salix (WT)	3Xa	10.2	419	1.050	0.042	23	0.54	5	0.82	27	0.94	18.6	0.82
Betula (dry)	**4B1a**	14.2	953	0.108	0.151	11	0.32	3, 1	0.61	30	1.07	25.4	1.70
Betula (dry)	**4B1b**	11.2	873	1.045	0.047	12	0.30	3, 1	0.54	31	0.9	22.7	1.46
Betula (WT)	4B2a	25.9	659	1.157	0.061	10	0.63	7	0.75	5	1.32	20.0	0.93
Betula (WT)	4B2b	8.6	644	0.293	0.097	11	0.25	3	0.69	25	0.85	24.7	1.39
Betula (WT)	4B3a	28.7	1000	0.100	0.166	10	0.54	7	0.80	10		18.9	0.93
Betula (WT)	4B3b	13.8	995	0.244	0.111	11	0.44	3, 1	0.44	27	0.75	22.9	0.98
Rubus	4R1a	16.0	441	0.230	0.122	11	0.25	5	0.30	18	1.53	17.7	0.54
Rubus	4R1b	8.3	342	0.824	0.084	11	0.29	6	0.80	22	1.08	21.9	0.88
Rubus	4R2a	29.9	694	0.103	0.179	11	0.50	7	0.82	8	2	20.3	0.73
Rubus	4R2b	16.6	637	0.602	0.108	12	0.19	6	0.73	19	1.49	23.3	0.97
Sedge	**4S1a**	26.9	998	0.191	0.159	20	0.46	6	0.83	11	0.76	22.0	1.05
Sedge	**4S1b**	14.9	716	0.273	0.127	13	0.20	1	0.82	30	0.62	21.3	0.92
Sedge	4S2a	14.1	300	0.970	0.062	11	0.55	5	0.80	10	0.87	21.9	0.93
Sedge	4S2b	14.8	740	0.387	0.101	13	0.28	3, 1, 4	0.73	32	0.86	26.0	1.23
Tussock	**4T2a**	13.8	979	0.103	0.173	10	0.41	3, 1	0.79	29	0.7	22.1	1.35
Tussock	**4T2b**	10.0	627	0.169	0.128	11	0.14	3, 1	0.49	27	0.75	18.8	0.73
Tussock	**4T3a**	9.9	388	0.296	0.107	13	0.51	3, 1	0.71	26	0.78	27.4	2.03
Tussock	**4T3b**	6.6	882	1.677	0.023	9	0.25	3, 1, 2	0.61	35	0.69	19.9	0.68
Tussock	**4T4a**	8.9	751	0.111	0.154	10	0.27	3, 1	0.67	26	0.69	26.8	1.94
Tussock	**4T4b**	9.4	670	0.276	0.094	12	0.15	3, 1, 2	0.30	30	0.62	17.3	0.57
Tussock	**4T5a**	11.1	281	0.174	0.146	6	0.29	3, 1, 2	0.52	37	0.53	28.2	2.25
Tussock	**4T5b**	7.7	402	1.074	0.047	10	0.22	3, 1	0.50	30	0.68	21.5	1.27
Salix (dry)	4X1a	15.8	448	0.231	0.120	22	0.73	5	0.81	5	1.72	19.9	1.03
Salix (dry)	4X1b	25.3	1000	0.960	0.085	12	0.35	4	0.79	15	1.0	21.1	1.04

Table 5. Continued

Vegetation Type	Code	P_{max}	k	R_b	β	n	RMSE	Generic Parameter Sets	Generic RMSE	Shared Parameter Sets	LAI	Mean Temp. (°C)	Mean VPD (kPa)
Salix (WT)	**4X2a**	30.0	726	0.356	0.134	11	0.67	7	0.80	5	1.59	23.2	1.08
Salix (WT)	**4X2b**	18.2	433	0.384	0.120	11	0.38	4	0.74	25	0.77	20.1	0.68
Salix (WT)	**4X3a**	22.7	999	0.892	0.065	9	0.50	5	0.82	15	1.95	16.9	0.61
Salix (WT)	**4X3b**	15.5	1000	0.293	0.125	11	0.25	3, 1, 4, 6	0.74	33	0.93	25.5	1.38

Parameters are generated by fitting observational data at each site and period to equation (3). P_{max}, k, R_b and β are fitted parameters. RMSE is the root-mean-square error of the fitting process for individual data sets. Generic parameter sets indicates which of the seven generic parameter sets (Table 6) generate a statistically acceptable description of the flux data for each light curve. The parameter sets are listed with the most generic (that is, commonest) parameter set first (Table 6). Generic RMSE indicates the root-mean-square error of the fitting process using the first of the listed generic parameter sets. Shared parameters sets indicates the number of other sites and periods that share acceptable model parameters. LAI is the leaf area index as determined by NDVI. Codes marked in bold indicate no significant differences in PIRT model parameters between periods for measurements at the same site.
WT, water track; n, number of flux measurements.

data. PS 5, with the second highest P_{max}, explained measurement sets in some wet tussock, *Rubus*, *Salix* and sedge tundra. PS 6 was required to explain the measurements at 4R1, 4R2 and 4S1 (sites which caused problems in the RT model due to low temperature range). PS 7, with the highest P_{max}, explained observations at some productive *Betula*, *Rubus* and *Salix* sites.

We looked for correlation between PIRT generic model parameters and other biotic and abiotic variables. We found a significant correlation between estimated P_{max} and LAI for all measurement sets ($n = 43$ for this and all cases below, $r^2 = 0.53$, $P < 0.001$, Figure 7). There were also significant, but weaker, correlations between P_{max} (generic parameters) and VPD ($r^2 = 0.13$, $P < 0.05$) and mean temperature ($r^2 = 0.12$, $P < 0.05$). Thus, site-level changes in temperature and light sensitivity of C dynamics could largely be explained by impacts on P_{max} caused by changes in LAI, primarily, and VPD and temperature, secondarily. The largest changes in LAI were identified at the *Salix* sites (4X1-3) and the *Rubus* sites (4R1-2). These sites all required different generic parameter sets to describe their light and temperature responses during the two measurement periods (Table 5). On the other hand, LAI changes at tussock sites were small (<0.2), and these sites had similar C dynamics during both time periods.

We expected that the apparent quantum yield (Q) would be similar among all sites and time periods, due to the shared C3 biochemistry. If this were true, then P_{max} and k would be linearly correlated ($Q = P_{max}/k$). We did find a significant linear correlation between P_{max} and k using all sites and time periods ($n = 43$) based on the individual parametrizations ($r^2 = 0.22$, $P < 0.01$) and generic parametrizations ($r^2 = 0.23$, $P < 0.01$). The relatively weak relationship (low r^2) between P_{max} and k probably arises from the flux measurements being undertaken at the canopy scale, where patterns of light interception and foliar geometry influence Q more strongly than on the leaf scale. We did not find any significant relationships between k and LAI or VPD or temperature.

We tried to incorporate LAI estimates into the PIRT model in a number of ways, to see if a single model parametrization could describe C sink strength along the toposequence, if LAI were included as a site descriptor. In method 1, we normalized all flux data by LAI estimates for each site and period. In method 2, we converted flux data to an estimate of gross photosynthesis using the RT model, and then normalized the photosynthesis estimate by LAI. And in method 3, we adjusted the

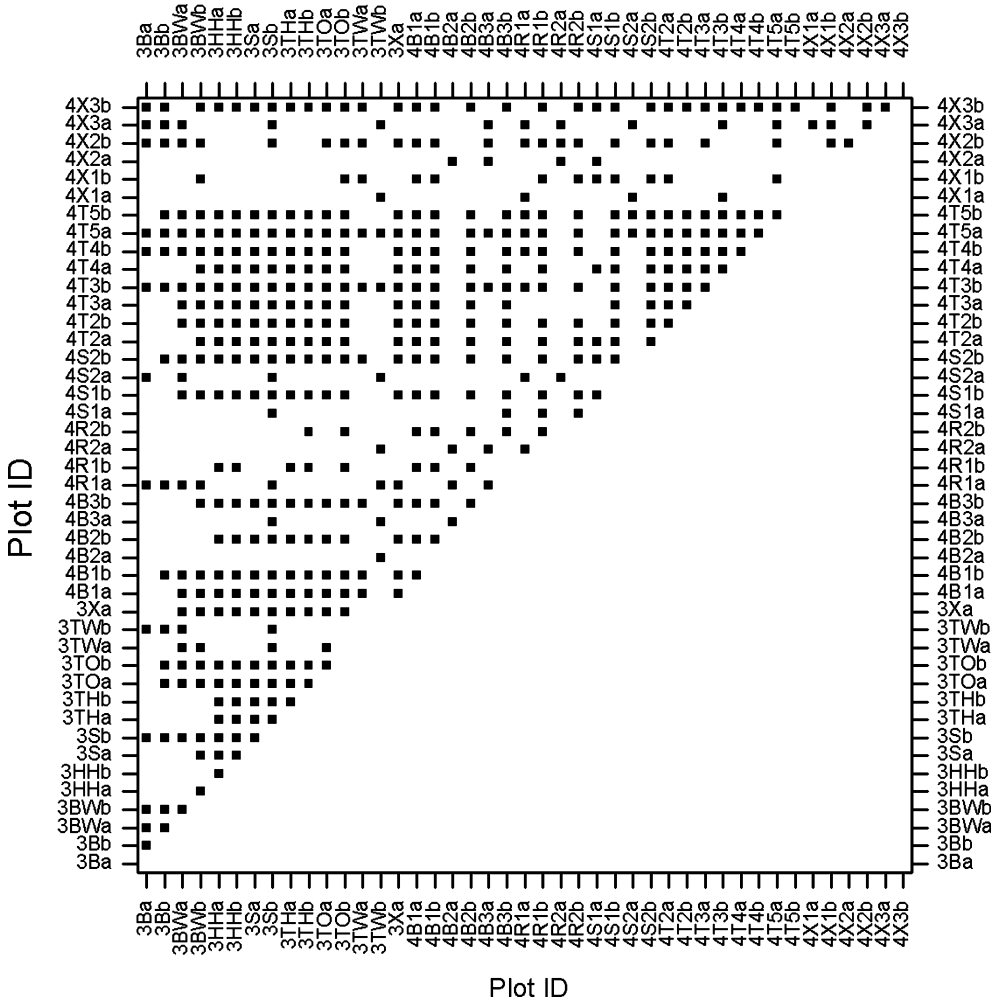

Figure 4. Common parameter analysis of the PIRT model for each site and each time period. *Symbols* indicate that a single parameter set in the PIRT model can acceptably predict C fluxes at both measurement sites and/or periods. The *lack of a symbol* indicates that no common parameters were found (significant at 95% level). Sites and periods are identified by plot ID code (see Table 1). The suffixes *a* and *b* indicate that measurements were from the first or second time period, respectively, for the site.

PIRT model to include LAI as a multiplier in the top half of the second term in equation (3). For each method, we found acceptable parameter combinations by the MLT, whereby the model could explain the observations of each data set (except the always difficult plot 2, period 2). However, after each experiment, we found that more parameter sets were required to describe the toposequence, rather than fewer. The cause of the increase in the number of parameter sets required for fitting the data is likely to be the uncertainty in the LAI data.

Analysis of Vegetation Data

The estimates of LAI show clear changes along the toposequence. LAI is highest in the foot-slope sites, *Salix* and *Rubus*, where soils are deeper and nutrient cycling is more rapid (Giblin and others 1991; Shaver and others 1996). In the saturated soils of the valley bottom, anaerobicity limits production, and reduces the LAI (sedge sites). Along the mid-slopes and upper-slopes, dominated by tussock tundra, LAI declines as soils thin and nutrient availability declines. The exception is in the water tracks that channel moisture down the valley sides, concentrating nutrients and supporting more productive vegetation (*Betula*).

We found that the data from the LAI-2000 were not suitable for predicting LAI in the vegetation types we sampled. There was a large positive intercept on the relationship between the LAI-2000 estimates of LAI and those derived by harvest. The problems with the equipment are likely connected

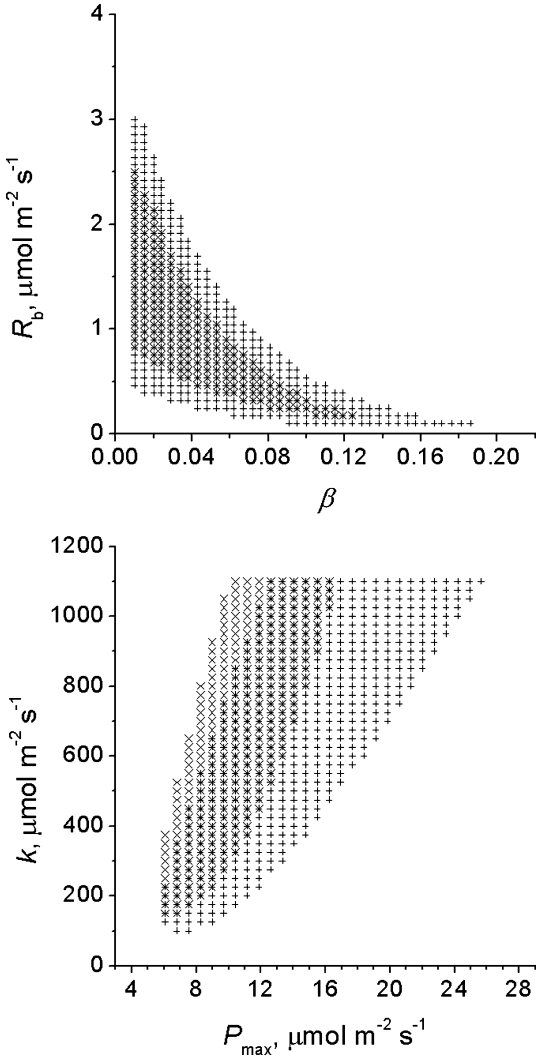

Figure 5. A comparison of acceptable parameters for the PIRT model applied to data collected at a sedge site during early July (3Sa, *cross symbol*) and late July (3Sb, *plus symbol*) 2003. *Symbols* indicate values of parameter sets that produce acceptable predictions of observations. The overlap in the parameters indicates no change in light and temperature responses of C dynamics.

to the low stature of much of the vegetation (van Wijk and Williams 2005).

Conclusions

Our research objective was to quantify the heterogeneity of landscape C dynamics within an arctic catchment. We have shown clear changes in species dominance and LAI along a toposequence. In so doing, we have identified surface reflectance measurements (NDVI) as most appropriate indirect technique for measuring LAI in Alaskan tundra. We have shown how a series of repeated ecosystem C flux measurements under irradiance manipulations can be used to distinguish significant differences in temperature and light responses of C cycling in low stature vegetation.

Table 6. Generic Parameter Sets for the PIRT Model

Generic Parameters	P_{max}	k	R_b	β	Number of Acceptable Curves
1	14.1	1000	0.535	0.076	18
2	17.0	825	0.172	0.129	8
3	9.7	550	0.39	0.086	23
4	14.8	625	1.622	0.043	6
5	17.7	500	0.39	0.1	5
6	11.9	525	0.897	0.081	4
7	25.7	725	2.928	0.024	4

P_{max}, k, R_b and β are fitted parameters. The total number of light curves for which each generic parameter set was acceptable is also shown.

Tussock tundra is the most abundant vegetation type in the pan-Arctic, and we found unchanging light and temperature responses during July and August measurements at six out of seven measured sites (the exception being a wet tussock tundra site on the foot-slope). Our analysis suggests a strong connection between this common behaviour and the small spatio-temporal variation in LAI of tussock tundra (mean ± SD 0.66 ± 0.16, n = 14). The most productive sites were *Rubus* and *Salix* dominated foot-slopes, and *Betula* back-slopes, during July. By August, in most cases, LAI had fallen in these sites, and there was a reduction in the estimated maximum photosynthetic rate, as determined from chamber measurements. These non-tussock sites are both structurally and functionally more diverse, temporally and spatially, than tussock tundra. Whereas all tussock sites can be described by a single temperature and light response surface, other vegetation types cannot be classified so simply. Over the spatial and temporal sampling we used, we found *Rubus* and *Betula* sites each required three distinct temperature and light response surfaces. Sedge and *Salix* both required four separate surfaces. This diversity of response within a single vegetation type complicates the construction of landscape estimates of C cycling. Our results suggest that in the northern foothills of the Brooks Range, at least, the growing season activity of tussock tundra can be simulated spatially using a single parametrization of a simple light and temperature response model. Non-acidic tussock tundra and alpine tundra may prove to behave differently (Walker and others 1998), and we sug-

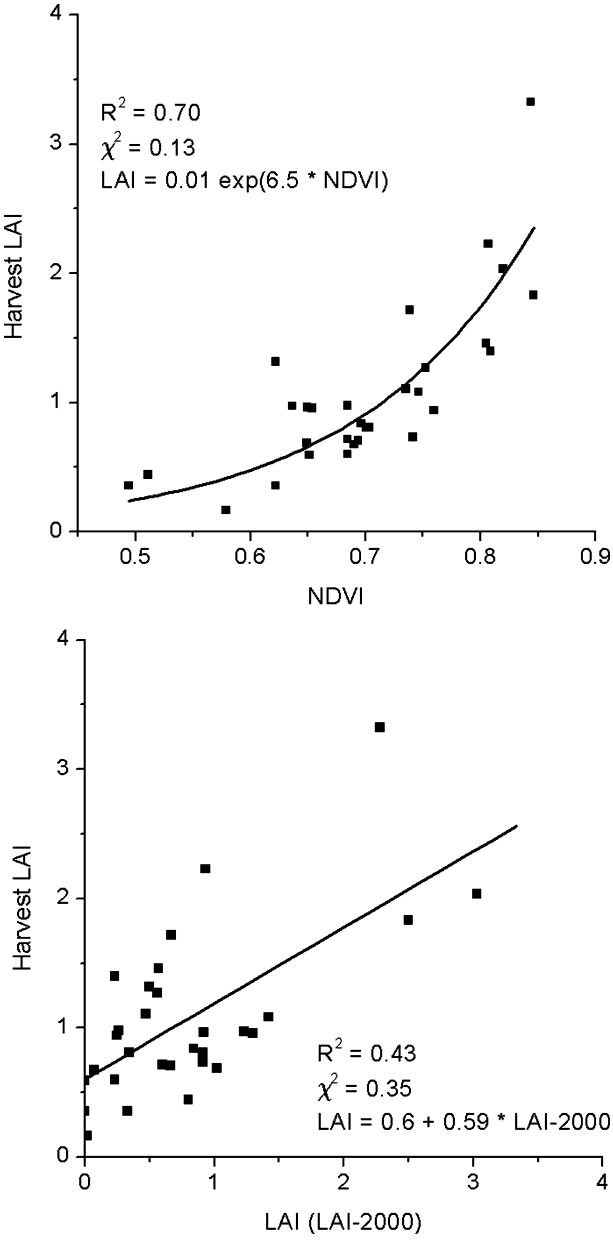

Figure 6. Correlation between harvested LAI and NDVI of 0.2 m × 0.2 m plots (*top*) or LAI-2000 of 0.2 m × 0.2 m plots (*bottom*). *Lines* shows the best model fit. $n = 30$.

gest testing this scaling approach in these other important tundra types as a possible course for future research. However, estimating the activity of non-tussock sites is not so straightforward, as vegetation type does not seem to be usefully predictive. Instead, estimates of LAI are more useful. We identified significant changes in C dynamics at some non-tussock sites during the growing season, and these are likely connected to observed alterations in LAI. This functional variability within the peak growing season emphasizes the importance of high temporal resolution LAI driver data for generating landscape predictions of C dynamics.

We have developed a methodology for determination of landscape heterogeneity, by finding functionally different landscape units. We have identified significant differences in C cycling within a small arctic catchment. This scale is considerably smaller than the size of the flux tower footprint, or the resolution of sensors such as MODIS. The next stage in this research is to explore how knowledge of variable C sink strength within a flux tower footprint, as shown here, can improve understanding of C cycling at the larger, footprint scale.

ACKNOWLEDGEMENTS

We acknowledge funding from the US National Science Foundation (Grant numbers OPP-0096523, OPP-0352897, DEB-0087046, and DEB-00895825). Also, we are grateful to Jim Laundre, Brooke Kaye, Beth Bernhardt and Åsa Rennermalm for assistance with the field work. We also thank Donie Bret-Harte for her advice on protocols.

REFERENCES

Baldocchi DD. 2003. Assessing the eddy covariance technique for evaluating carbon dioxide exchange rates of ecosystems: past, present and future. Glob Change Biol 9:479–92.

Giblin AE, Nadelhoffer KJ, Shaver GR, Laundre JA, McKerrow AJ. 1991. Biogeochemical diversity along a riverside toposequence in Arctic Alaska. Ecol Monogr 61:413–35.

Gurney KR, Law RM, Denning AS, Rayner PJ, Baker D, Bousquet P, Bruhwiler L, Chen YH, Ciais P, Fan S, Fung IY, Gloor M, Heimann M, Higuchi K, John J, Maki T, Maksyutov S, Masarie K, Peylin P, Prather M, Pak BC, Randerson J. Sarmiento J, Taguchi S, Takahashi T, Yuen CW. 2002. Towards robust regional estimates of CO_2 sources and sinks using atmospheric transport models. Nature 415:626–30.

Hinzman LD, Kane DL, Gieck RE, Everett KR. 1991. Hydrologic and thermal properties of the active layer in the Alaskan arctic. Cold Reg Sci Technol 19:95–110.

McFadden JP, Eugster W, Chapin FS III. 2003. A regional study of the controls on water vapor and CO_2 exchange in arctic tundra. Ecology 84:2762–76.

Oechel WC, Hastings SJ, Vourlitis G, Jenkins M, Riechers G, Grulke N. 1993. Recent change of Arctic tundra ecosystems from a net carbon dioxide sink to a source. Nature 361: 520–3.

Oechel WC, Vourlitis GL, Hastings SJ, Zulueta RC, Hinzman L, Kane D. 2000. Acclimation of ecosystem CO_2 exchange in the Alaskan Arctic in response to decadal climate warming. Nature 406:978–81.

Shaver GR, Billings WD, Chapin FS III, Giblin AE, Nadelhoffer KJ, Oechel WC, Rastetter EB. 1992. Global change and the carbon balance of Arctic ecosystems. BioScience 42:433–41.

Shaver GR, Laundre JA, Giblin AE, Nadelhoffer KJ. 1996. Changes in live plant biomass, primary production, and spe-

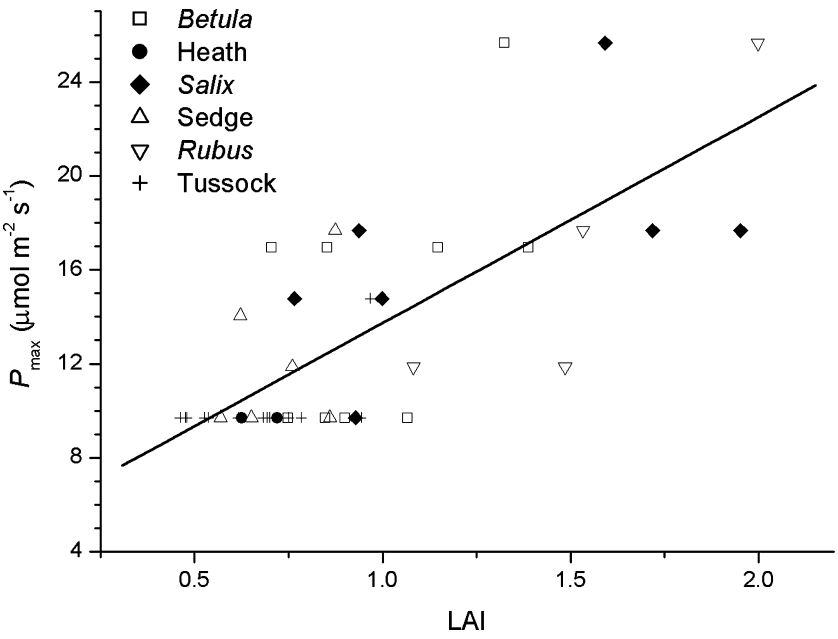

Figure 7. Correlation between estimated maximum photosynthetic rate and measured leaf area index. The vegetation type of each plot is indicated by *symbol*, as indicated in the legend.

cies composition along a riverside toposequence in arctic Alaska, USA. Arct Alp Res 28:363–79.

Shaver GR, Bret-Harte SM, Jones MH, Johnstone J, Gough L, Laundre J, Chapin FS. 2001. Species composition interacts with fertilizer to control long-term change in tundra productivity. Ecology 82:3163–81.

Stieglitz M, Giblin A, Hobbie J, Williams M, Kling G. 2000. Simulating the effects of climate change and climate variability on carbon dynamics in Arctic tundra. Glob Biogeochem Cycles 14:1123–36.

Vourlitis GL, Oechel WC. 1997. Landscape-scale CO_2, H_2O vapour and energy flux of moist-wet coastal tundra ecosystems over two growing seasons. J Ecol 85:575–90.

Vourlitis GL, Oechel WC. 1999. Eddy covariance measurements of CO_2 and energy fluxes of an Alaskan tussock tundra ecosystem. Ecology 80:686–701.

Vourlitis GL, Oechel WC, Hope A, Stow D, Boynton B, Verfaillie J, Zulueta R, Hastings SJ. 2000. Physiological models for scaling plot measurements of CO_2 flux across an arctic tundra landscape. Ecol Appl 10:60–72.

Walker BH. 1994. Landscape to regional-scale responses of terrestrial ecosystems to global change. Ambio 23:67–73.

Walker DA, Walker MD. 1996. Terrain and vegetation of the Imnavait Creek watershed. In: Reynolds JF, Tenhunen JD, Eds. Landscape function and disturbance in arctic tundra. Berlin Heidlberg New York: Springer, p 73–108.

Walker MD, Walker DA, Auerbach NA. 1994. Plant communities of a tussock tundra landscape in the Brooks Range Foothills, Alaska. J Veg Sci 5:843–66.

Walker DA, Auerbach NA, Bockheim JG, Chapin FSI, Eugster W, King JY, McFadden JP, Michaelson GJ, Nelson FE, Oechel WC, Ping CL, Reeburgh WS, Regli S, Shiklomanov NI. Vourlitis GL. 1998. Energy and trace-gas fluxes across a soil pH boundary in the Arctic. Nature 394:469–72.

van Wijk MT, Bouten W. 2002. Simulating daily and half-hourly fluxes of forest carbon dioxide and water vapor exchange with a simple model of light and water use. Ecosystems 5:597–610.

van Wijk MT, Williams M. 2005. Optical instruments for measuring leaf area index in low vegetation: application in arctic ecosystems. Ecol Appl 15:1462–1470.

Williams M, Eugster W, Rastetter EB, McFadden JP, Chapin FS III. 2000. The controls on net ecosystem productivity along an arctic transect: a model comparison with flux measurements. Glob Change Biol 6:(suppl 1)116–26.

Williams M, Rastetter EB, Shaver GR, Hobbie JE, Carpino E, Kwiatkowski BL. 2001. Primary production in an arctic watershed: an uncertainty analysis. Ecol Appl 11:1800–16.